Journal of
Oceanography and Marine Research

Marks, Oceanography 2014, 2:4
DOI: 10.4172/2332-2632.1000128

Research Article Open Access

Bubble Rotational Features – Preliminary Investigations

Roman Marks*

Institute of Marine and Coastal Sciences, University of Szczecin, Poland

Abstract

Photography experiments dedicated to explore the formation of bubble bottom vortex revealed that rising bubbles may develop even three types of rotational motion. A clockwise (CW) rotational motion is assembled within the bubble upper half sphere, a counter clockwise (CCW) rotary is developed within the bottom half sphere and a spliced (CW/CCW) bi-rotary motion can be assembled at the bubble equator or within the bubble vortex. Other experiments indicated that displacement of ions within the bubble spherical curvatures results in gathering of anions within the upper bubble half sphere, while the rotational grouping of cations prevail within the bubble bottom half sphere and its vortex. The merging and splicing of both oppositely directed and oppositely charged bubble rotational motions, resulting in assembly of ionic double helix motion, indicate that rising bubble rotational features are very akin to the architecture of RNA/DNA molecules. Thus, the matching properties of rising bubble bi-polar and bi-rotary features and architecture of RNA/DNA molecules are compared.

Keywords: Air-bubbles; Bubble vorticity; Bubble double helix, RNA/DNA molecules

Introduction

Bubbles generated in the sea surface waters during moderate and high wind speed conditions create whitecaps at the sea surface and produce sea salt aerosols [1-7]. During the rise in the water column bubbles also selectively scavenge some water constituents that enrich the sea surface micro layer [8,9] and sea derived aerosols [4,10,11].

The production of bubbles in the water intensifies with the increase in wind speed [12-14]. In addition, field and laboratory experiments confirmed that the production of bubbles in sea water and the related generation of sea-derived aerosol droplets increase with the degree of dissolved gases supersaturation [15,16].

Bubbles in the surface waters are mainly produced by breaking wave events, which are generated by the overturn of unstable wave crests [2,18]. However, the most enhanced production of bubbles and related generation of sea salt aerosols occurs under rainy and windy weather conditions [19].

Typical breaking wave-induced attenuation depth of bubbles in the sea surface water is c. 1 m [20,21] while rain droplets attenuate bubbles to the depth of c. 20 cm [12]. The size of the breaking wave mediated bubbles in the oceanic water ranges from about 1 μm to a few mm in radius, although their average occurrence radius is about 25 μm [21].

The depth of bubble dispersion in the water column increases with growing water temperature [21]. Immediately after dispersion in the water column, bubbles tend to rise according to their volume related buoyancy. During the rise in the water column, bubbles may gradually grow in size, especially under the conditions of supersaturation with respect to dissolved gases [16].

The speed of rising bubbles significantly differs between the so-called "dirty" (loaded with scavenged materials) and "clean" bubbles, as defined by Woolf and Thorpe [22]. The reported values range from 0.6 cm/s for "dirty bubbles" to 2.1 cm/s for "clean bubbles" of 0.1 mm radius and increase respectively to 4.8 cm/s for "dirty" and 8.5 cm/s for "clean" bubbles of 0.4 mm radius under water temperature of 10°C.

At the relatively "clean" water surface, single bubbles instantly burst ejecting a few large jet droplets of a micrometer size range and hundreds of small film droplets of sub-micrometer sizes [2,3,6,7,15]. Under such conditions, sea-derived droplets supply the troposphere with a variety of materials, including sea salt particles, providing condensation nuclei with an electric charge [12].

In the initial stage, the work has been dedicated to explain a process responsible for bubble mediated selective scavenge of bacteria in sea water [25]. During the experiments the bubble bottom vortex formation has been documented, but in addition an intriguing ability of rising bubbles to induce bi-ionic and bi-rotating motion has been discovered. Further experiments allowed distinguishing bubble tracers that perform a clockwise rotational motion, a counter clockwise motion and a spliced double helix like, bi-rotary motion. These findings offered to state a new concept of rising bubble rotational principles, which is introduced in. Since, the rising bubble rotational features showed very akin properties to spiraled molecules like RNA/DNA, a preliminary list of similarities is presented in.

Methods

Several laboratory experiments were undertaken to investigate the rising bubble rotary. In order to trace the bubble transcripts in the water column a photographic method was applied. The best photographs of bubble tracers were collected during the experiments with the use of a small glass cylinder of 50 ml volume under the condition of light illuminating from below the vessel (Figure 1).

During the experiments bubbles were generated in natural sea water or in artificial sea water by the effervescence method using a small (c. 1/10 of Salt Ems factitium (SEf) pill; by adding a small amount of sea salt or by adding 0.5 ml of CO_2 supersaturated water. Uniform-

***Corresponding author:** Roman Marks, Institute of Marine and Coastal Sciences, University of Szczecin, ul. Mickiewicza 16, 70-383 Szczecin, Poland, Tel: +48 91 444 25 30; Fax: +48 91 444 25 31; E-mail: marks@univ.szczecin.pl

Received October 24, 2014; **Accepted** November 25, 2014; **Published** December 01, 2014

Citation: Marks R (2014) Bubble Rotational Features – Preliminary Investigations. Oceanography 2: 128. doi: 10.4172/2332-2632.1000128

sized bubbles of 1 mm in diameter were produced by glass capillary aerators (Figure 1).

The transcripts of bubbles were recorded by a digital Canon 350D camera, with EFS 18-55mm lens, enhanced by 8 dioptric power lenses or by the lens with reverse ring. Macro photographs were taken using Tamron Xr Di 28-75 lens deployed with a reverse ring. The bubble-mediated rotational motion was typically captured and visualized in pictures taken with 1/15, 1/20 or 1/30 second shutter time.

It has to be explained, that all recorded transcripts of free rising bubbles in the water column, visualize a superimposition of at least two interacting rotational motions, taking place at the bubble wall and its vortex simultaneously. This is the reason, why the captured transcripts have rather blurry contours.

The recorded transcripts of rising bubble tracks (Figures 2, 4, 6 and 7) were scaled (Figure 1) in order to determine bubble diameter (d) in mm, the speed of bubble rise (V) in mm/s (calculated from the length of recorded bubble track, divided by the camera shutter time). Among the rotational properties: the number of recorded helical circuits (N) in 1/s, and related pitch (P) in mm as well as a linear velocity of spiraling circuits (Vc) in mm/s were derived. The values of (Vc) were calculated from the following equation:

$$Vc=d\pi N. \quad (1)$$

Where: $\pi=3.1416$.

The direction of rotary assembled within the bubble bottom hemisphere was indirectly determined through the effects induced by streams of jet droplets produced by bursting bubbles, collected on the rotary detection disk made of light cotton or polyurethane foam. The same direction of rotary was also induced by considering the slope of bubble circuits. In that sense, the bottom bubble circuits, characterized by larger pitch, were relatively more visible, thus it was easier to sense the direction of that rotary. All the reported experiments were performed in the Northern Hemisphere.

Bubble upper half sphere circuits with clockwise rotary

The bubble upper half sphere rotational circuits were easily detectable, since these form outer spirals, thus they are directly visible in the photos (Figure 2). This rotary motion forms relatively large diameter circuits of a smaller pitch as compared with bubble bottom half sphere circuits. For instance, a recorded bubble of diameter d=0.4 mm, produced by fuzzy salt at the water temperature of Tw=30°C and salinity of S=35‰ assembled c. 21 circuits in 1/15 second, which means it could assemble c. 20,000 circuits in a 1 m rise. In the captured transcript, also an internal rotating system assembled within the bottom half sphere can be seen as an internal core, although its features are covered by outer circuits (Figure 2).

By comparison with bottom bubble rotational features it is inferred that the upper half sphere develops and gathers a prescribed rotational motion in clockwise (CW) direction, although the direction of that sphere rotary was not measured yet. Probably, the rotary assembled within the bubble upper half sphere results from the displacement and acceleration of spherical hydrates and molecules intercepted into the spherical curvature of a bubble. It is assumed that, relatively heavier anions are probably more resistant to sudden displacement, thus these are successively accumulated within the upper bubble hemisphere. As a result the bubble upper half sphere gathers a prevailing negative charge. The net negative charge was confirmed by means of experiments devised to collect film droplets derived from the upper bubble cap during the bubble burst. These were collected on positively charged glass plate (Figures 1 and 3).

Bottom bubble half sphere circuits with counterclockwise rotary

In general, it is assumed that, if the rise speed of bubble is faster than the laminar motion, it results in reduction of hydrostatic pressure at the bubble bottom and accelerates displacement of ions and molecules at the bubble spherical curvature, thus it generates rotational features. In order to reveal the motion assembled within and under the bubble bottom half sphere, the rise speed of bubbles was increased, to force divergence of the upper hemisphere rotational circuits. It was noted that such divergent motion is more typical for bubbles larger than 0.3 mm.

After exceeding, the so-called critical speed, a bubble move fast enough to diverge the upper sphere circuits and reveal the bottom ones, which otherwise would be covered. For example, a captured bubble of d=0.375 mm rising in artificial seawater at Tw=55°C and S=35‰ with the speed of 33 mm/s perform c. 300 circuits per sec. of 0.11 mm pitch, spiraling with the speed of c. 353 mm/s at the helix wall (Figure 4). In order to compare both, that is: the upper and the bottom bubble hemispheric rotational parameters, the values of Vr, P, N, Vc are listed along with the direction of rotary of two bubbles of approximately the same diameter (Figure 4). It indicates that the rotary circuits developed at the bubble bottom hemisphere (tracer 1) are characterized by relatively higher rise speed, larger pitch and slightly reduced rotational speed at cylindrical tracer, as compared with the bubble of the same diameter but sustaining both rotaries, i.e. upper and the bottom ones (tracer 2).

The counterclockwise (CCW) direction of the bubble bottom half sphere rotary was inferred from the slope of recorded circuits (Figure 4, tracer 2). In addition, the (CCW) direction of rotary was confirmed by other sets of experiments dedicated to detect the rotary induced by a stream of jet droplets collected by the rotary detection discs made of ultra-light cotton and foam.

Other set of experiments using electrostatically charged plates exposed at the place of bubbles burst, confirmed that jet droplets derived from the bottom bubble sphere and bottom vortex contain a prevailing share of cations (Figures 1 and 5). The same, i.e. net positive charge of sea derived aerosols was previously reported by [12].

Bubble double helix

An especially interesting case has been observed when both CW

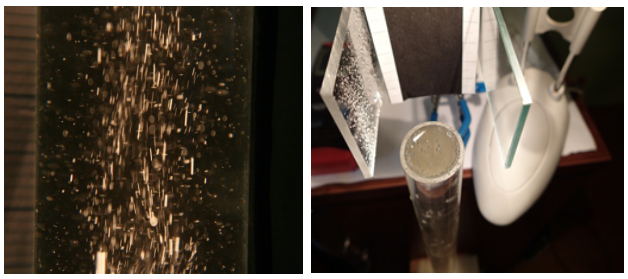

A B

Figure 1: Setups used to trace bubble rotary using an illuminated glass cylinder (A) and to investigate the bubble-mediated separation of ions, ejected by bursting bubbles and collected on negatively charged Plexiglas and positively charged glass plates, respectively (B).

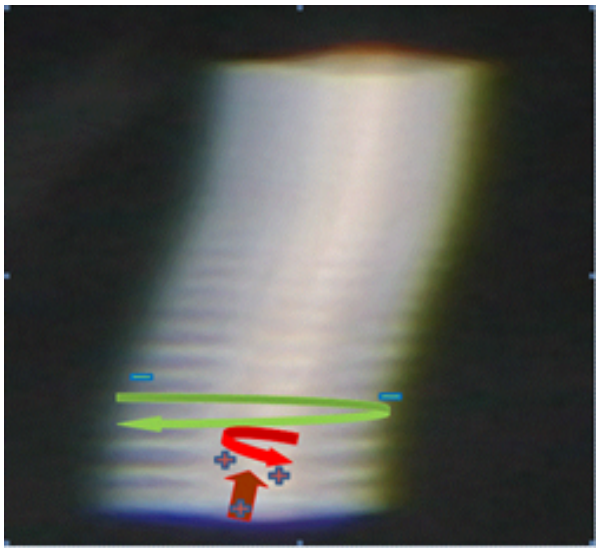

Figure 2: The image tracks the effervescence bubble of c. 0.4 mm in diameter during its rise in 1/15 second time; performing clockwise circuits i.e. 300 circuits per second of 0.06 mm pitch, spiraling with the speed of 377 mm/s at the helix wall, around almost vertical axis of rotation. Inside the tracer, internal helical motion derived from the bubble bottom vortex can be seen. In addition, the electric charge of ions incorporated into both: upper (anionic) and bottom (cationic) half spheres is marked. The bubble was produced in artificial sea water by fuzzy salt at Tw = 30 ˚C and S = 35‰.

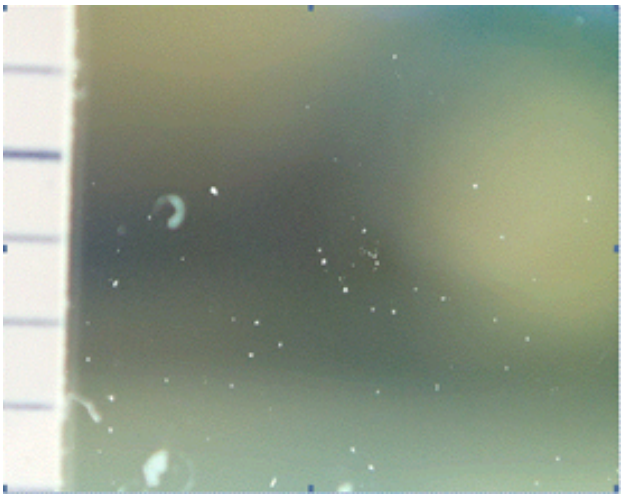

Figure 3: Residues of small film droplets containing dominating share of anions collected on the positively charged glass plate during the experiments dedicated to identify the bubble mediated separation of ions. Stream of uniform in size bubbles of d = 1 mm were produced in natural sea water by glass capillary. In the left side a scale with a mark of 1 mm is visible.

and CCW rotaries merged forming "empty cylinder traces, with visible (×) marks" as seen in Figure 6. It indicates that under specific conditions both rotaries may merge and interlace theirs polarized directions of rotary and polarized ionic content. Such cases were assembled more typically by relatively small effervescence bubbles under water temperature ranging from 25°C to 40°C and salinity ranging from 30‰ to 36‰. The observed evidence indicates that bubbles may coherently marge and assemble oppositely directed rotaries of a double helix-like architecture. The merged, preassembled bubble rotaries form "empty" cylindrical tracers, with typical "x" marks, as can be seen in Figure 6 (left tracer).

It has to be explained that the double helix splicing might be inevitable at the bottom bubble cavity, after the collapse of previously assembled bi-rotational circuits, as for instance captured in Figure 7. It is anticipated that the convergence of both rotaries towards the center of bubble bottom funnel cavity forces hyper-strong Pirouette effect. During that phase, the reduction of funnel scale decreases also the dimension of emerged rotaries to the smallest possible sizes that is possibly to molecular sizes. Considering for example the two bubbles of d=0.375 mm captured in Figure 4, its potential reduction to nm sizes that is typical for DNA will be of 10^{-5} range. Thus the roughly calculated number of circuits per seconds due to cavity reduction will increase to $N \cdot 10^5$ that is to 300×10^5 and 375×10^5 per second respectively for two scaled bubbles, if for simplicity, non viscous motion of bubbles in the water will be consider. At this stage of experimental approach, it should be mentioned that there is still much that we do not know about bubble rotational motion, but especially about dissipation of rotational features in the sub-babble cavity.

Discussion

At this stage of research, the observations made suggest that bubbles rising in salty waters induce at least five of the following interacting properties: positive and negative electrostatic polarity, clockwise and counterclockwise directed rotary as well as enrichment of hydrophobic matter. These allow combining the synergic processing of matter incorporated into the three bubbles mediated rotational features: 1) the prevailing collection of anions within the bubble upper hemisphere; 2) the prevailing collection of cations within the bubble bottom vortex; as well as 3) selective drawing of hydrophobic material into the low pressure bottom vortex. Experiments confirmed that especially efficient collection, in terms of dissolved and suspended matter, occurs at the bubble bottom vortex. Considering the findings, it is suggested that the drawing of dissolved gasses [6,16] forms the bubble bottom upper layer and successively increases the bubble volume; the drawing of hydrophobic matter [10,11,25] composes a vortex middle layer, while the gathering of cations [12] forms a bottom vortex layer ("water panel" in Figure 8).

After the waterborne processing is completed, the matter is immediately transferred to air, where further airborne processing takes place (Figure 8).

It has to be underlined that further effort to explore the bubble rotational features in salty waters is needed. Among processes that need particular attention is a potential of rising bubbles to undergo splicing of bi-rotating motion at the wave slope. In addition, a set of similar investigations has to be completed in the Southern Hemisphere. Beside the experimental effort, a modeling and recently developed visualization techniques, that are applicable to indicate bubble rotation [23] should be developed. However, if the stated concept is correct, it may have extended impact on the overall chemistry, biology and medicine related research.

Similarities between rotational properties of bubbles and RNA/DNA

Since the bubble mediated bi-rotational and bi-ionic motion display akin features to the RNA/DNA architecture, and each single bubble organizes extremely precise rotational motion and splicing of matter, both bubble and RNA/DNA rotational systems are compared.

First of all, it is worth mentioning that the dissipation of below bubble rotaries may compress the rotaries and narrow the diameter of spiraled circuits even to a molecular size. Moreover, the sub-bubble

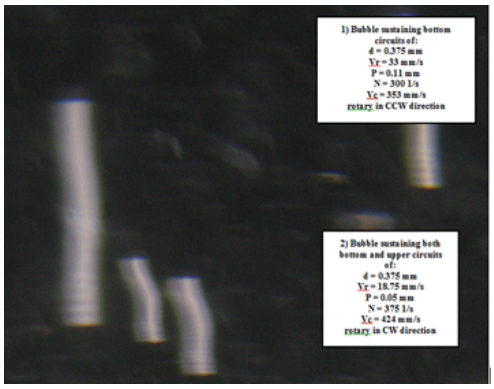

Figure 4: Comparison of two similar bubbles of d = 0.375 mm: 1) sustaining only bottom circuits and 2) sustaining both the upper and bottom circuits, rotating around the vertical axis in term of: rise speed (Vr), their pitch (P), number of circuits per second (N) and speed of rotation (Vc). Picture was taken in 1/15 second, at *Tw*=55 ˚C, *S*=35‰; bubbles were produces in artificial sea water by (SEf).

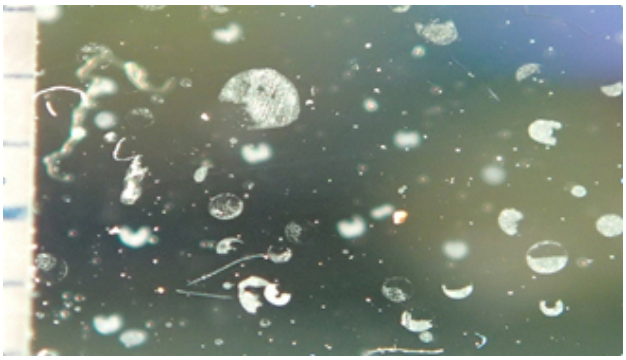

Figure 5: Residues of large jet droplets derived from bubble bottom vortex, containing dominating share of cations, collected on the negatively charged Plexiglas plate during the experiments dedicated to detect the bubble mediated separation of ions. The stream of bubbles of d=1 mm was produced in seawater by capillary aerator. The visible scale mark is 1 mm.

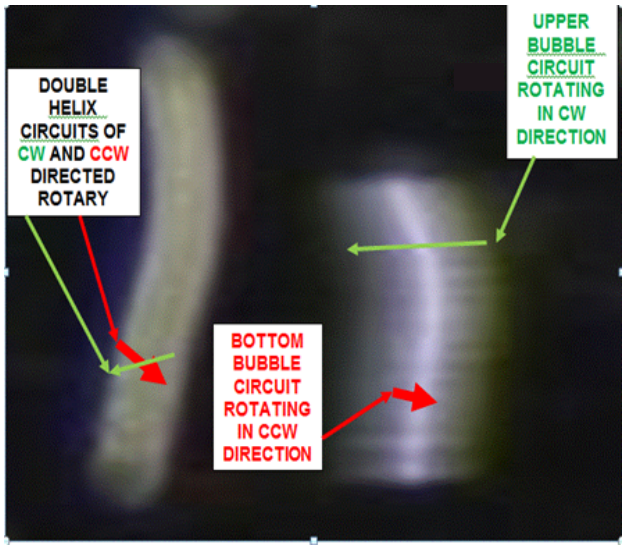

Figure 6: The merged upper and bottom half spheres helical motions, rotating around the vertical axis, forming double-helix empty cylinder with "x" marks (left tracer) of *d*=0.18 mm; and bubble before the merging (right tracer) of *d*=0.36 mm in diameter, forming outer (upper) rotational coils covering internal (bottom circuits). The experiment was conducted at *Tw*=30 °C and *S*=30 ‰; bubbles were produced by using the effervescence fuzzy salt.

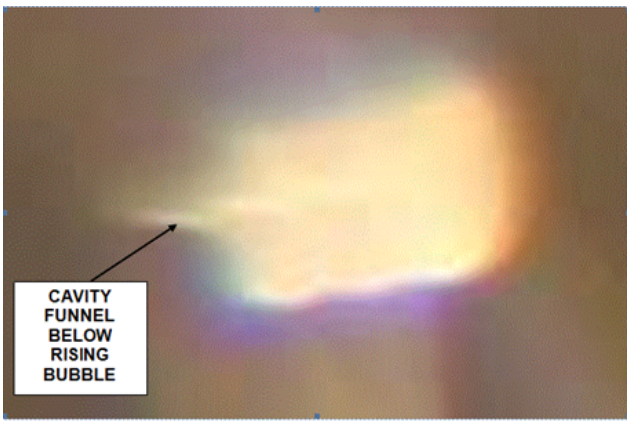

Figure 7: Spherical cavity funnel, rotating around almost horizontal axis, formed below bubble of 0.18 mm diameter, rising in water under Tw=41.4 ˚C i S=8‰. Bubble was produced by (SEf). Picture was taken by Tamron Xr Di 28-75mm lens with reverse ring, in 1/30 s time.

rotary can be assembled and continued in a water column even for tens of meters (although not confirmed yet). Secondly, the rising bubbles indicate that bubbles dissipate a high amount of energy by means of a rotational motion. Thirdly, bubble bottom vortex collects hydrophobic matter that can stabilize internal structures of molecules, if eventually assembled. Thus, the remnants may likely leave stretches capable of replicating precise (spiraled) motion and being very similar to the architecture of RNA/DNA molecules.

In order to state the anticipated similarities, the matching properties of bubble bi-polar and bi-rotary motions and architecture of RNA/DNA molecules are compared in (Table 1).

Subsequently, the preliminary comparison of both systems indicates that rising bubbles and RNA/DNA molecules demonstrate at least three very similar properties, namely: 1) bi-rotational spirals; 2) bi-electric lined-stretches, and 3) substantial, internal enrichment of hydrophobic materials. These surprising coherences, along with the capability of bubbles to assemble almost unlimited (hyper large) number of precise coils, allow to anticipate that the bubble and related bubble-to-aerosol system of matter processing may provide unique mechanism able to generate a bi-rotary and bi-ionic motion that can setup spiraled and be-spiraled molecules. In addition, the molecules may likely "memorize" the motion which can be replicated by means of activating a precise bi-rotary/bi-ionic system of precise spiraled motion. In particular, the continuous formation of the bubble bottom vortex that renews its cationic domain as well as collects hydrophobic matter and then compresses rotating upper and bottom bubble coils to molecular domains, plays the most important role, which involves both initiating and organizing activities. However, there is much about rotary of ions as well as bubbles in salty waters that we still do not know.

Finally, the bubble mediated organization of dissolved inorganic matter by means of rotational-electrostriction is elucidated. Thus, the previous concepts of matter synthesis on the primitive Earth, envisioned by [24] as well as the concept of "bubblesol" origin of life are directly supported. The principles of matter synthesis may base on bubble induced synergic processing that combine: the separation of anionic and cationic matter, rotational organization of bi-ionic stretches, providing isolating domain for polar basis and extreme rotational condensation of matter. The hyper abundant and continuous processing of matter in the euphotic column of oceanic

Rotational features	Bubble properties	RNA/DNA features
Counterclockwise helix (CCW)	Formed at bottom cationic half sphere and vortex	(CCW) basis, positively charged, cationic
Chemical composition	Selected cationic compounds as: Na, Mg, Ca, K	Adenine, Cytosine and outer backbone of 6 Å slot
Clockwise helix (CW)	Formed at anionic upper half sphere	(CW) basis, negatively charged, anionic
Chemical composition	Selected anionic compounds as: Cl, Sulfates, Phosphates	Guanine, Thymine, outer backbone of 12 Å slot
Double helix (CW/CCW)	Spliced opposite directed bi-helical motion	DNA, opposite (CCW/CW) electrically polar bones
Chemical composition	Preselected water components	Two antiparallel backbones
Internal Core (CCW)	Formed under the bubble and inside its bottom vortex	Hydrophobic core inside RNA/DNA of (CCW)
Chemical composition	Preselected hydrophobic water components enriched by C, N, P,O	Hydrophobic matter, filling space between polar bones

Table 1: Preliminary list of similarities between the rotational properties of bubbles and the RNA/DNA features.

water may likely result in extremely abundant assemblies of spiraled matter, especially in the tropical oceans. Since, the matter processing mechanisms are governed by the same set of physical principles; these might be responsible for assembly of coherent spiraled matter in a geological time scale. Thus bubble induced, rotational ionic activities might be responsible for initiating and forcing viability (i.e. rotary motion of ions) in bio cells, as well as inducing steady and coherent evolution of spiraled matter on the Earth.

Conclusions

The outlined experiments allow drawing the following general conclusions:

1. Bubbles rising in seawater displace molecules with accelerated speed, inducing bi-directed rotational motion of ions; experiments conducted in the Northern Hemisphere indicated that a clockwise rotational motion of anionic domain is gather at the bubbles upper half sphere, while a counterclockwise motion of stronger cationic domain is gather within the bottom half sphere and its vortex (Figure 8).

2. Large bubbles of c. (d>0.3 mm) rise with relatively high speed, thus they typically shed the upper hemisphere rotational motion and keep only a bubble bottom circuits.

3. Small bubbles of c. (d ≤ 0.3 mm) rise with relatively slow speed, thus they may sustain both the bubble upper and the bottom hemisphere motions and eventually interlaces both rotaries within the bubble vortex-cavity or at the bubble equator.

4. The bubble's upper hemisphere motion forms larger diameter anionic circuits of relatively smaller pitch, rotating along the bubble equator.

5. The bubble's bottom hemisphere motion forms relatively smaller diameter cationic circuits of a larger pitch, which rotates around the bubble bottom and in its vortex.

6. Cationic domains gathered within the bottom bubble sphere form strong lined-up chains, that probably enforces electrostriction of anions, within the bubble upper sphere.

7. Under water temperature above 20°C, a spontaneous splicing of both rotaries, forming a double helix motion may take place.

8. Probably unavoidable splicing of both rotaries takes place within the bottom cavity vortex, when both of the previously assembled bubble rotaries collapse.

9. The collected evidence suggests that bubble mediated anionic, cationic and hydrophobic domains may interlace and assemble motion of RNA/DNA like architecture, thus the bubble induced rotational features might be considered as an unique and extremely efficient, synergic mechanism responsible for spiraled matter creation as well as its coherent evolution taking place in salty waters on the Earth.

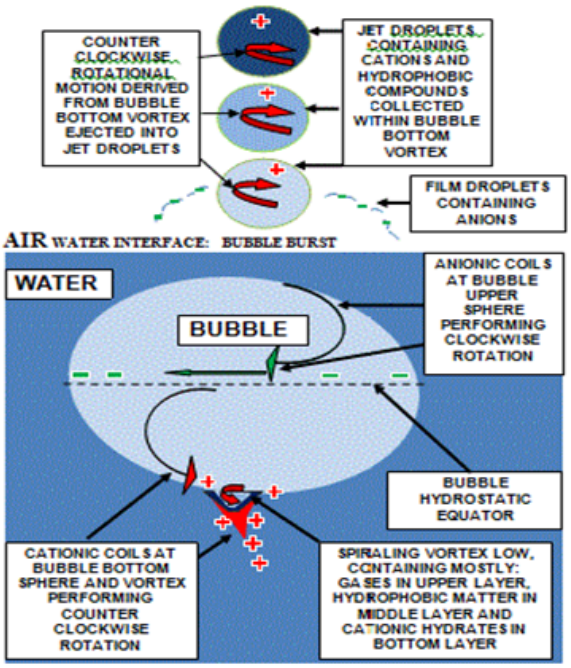

Figure 8: A general concept of a rising bubble in salty water in the Northern Hemisphere with marked upper and bottom half sphere rotational motion and related ionic separation as well as bottom vortex layers partitioned into: gaseous compounds (upper layer), hydrophobic matter (middle layer), cationic hydrates (bottom layer); the related transition of vortex materials into jet droplets and dissipation of counter clockwise rotary derived from bottom vortex is marked.

10. Bubble induced bi-rotational motion and its transition into aerosol droplets may provide synergic mechanism able to select and process dissolved matter and crate bio-cells.

References

1. Blanchard DC, Woodcock AH (1957) Bubble formation and modification in the sea and its meteorological significance. Tellus 9: 145-158.
2. Monahan EC (1971) Oceanic whitecaps. J. Physical Oceanography 1: 139-144.
3. Lovett RF (1978) Quantitative measurements of airborne sea salt in the North Atlantic. Tellus 30: 350-364.

4. Liss PS, Slinn WGN, Reidel D (1983) Gas transfer: experiments and geochemical implications in air-sea exchange of gases and particles. 108: 241-298.

5. Wu J (1986) Whitecaps, bubbles, and spray. Oceanic Whitecaps Monahan EC and Mac Niocaill G (Eds) 2: 113-124.

6. Sinha V, Villiams J, Meyerhöfer M, Riebesal U, Paulio AI, et al. (2007) Air-sea fluxes of methanol, acetone, acetaldehyde, isoprene and DMS from a Norwegian ford following a phytoplankton bloom in a mesecosm experiment. Atmos Chem Phys 7: 739-755.

7. Bigg EK, Leck C (2008) The composition of fragments of bubbles bursting at the ocean surface. J Geophys Res 113: 209.

8. MacIntyre, F (1974) The top millimeter of the ocean. Scientific American, 230, 62-77.

9. Vanninkof R (1992) Relationship between wind speed and gas exchange over the ocean. J Geophys Res 97: 7373-7382.

10. Blanchard DC, Syzdek L (1970) Mechanism for the water-to-air transfer and concentration of bacteria. Science 170: 626-628.

11. Aller JY, Kuznetsova MR, Jahns CJ, Kemp PF (2005) The sea surface microlayer as a source of viral and bacterial enrichment in marine aerosol. J Aerosol Science 36: 801-812.

12. Blanchard DC (1963) Electrification of the atmosphere by particles from bubbles in the sea. Progress in Oceanography 1: 73-197.

13. Monahan EC, Fairall CW, Davidson KL, Boyle PJ (1983) Observed intr-relations between 10 m winds, ocean whitecaps and marine aerosols. Quartaly Journal of the Royal Meteorology Society 109: 379-392.

14. Callaghan A, de Leeuw G, Cohen L (2007) Observations of Oceanic Whitecaps coverage in the North Atlantic during Gale Force Winds. Nucleation and Atmospheric Aerosols. Colin D, O'Dowd and Paul EW (Eds) 1088-1092.

15. Stramska M, Marks R, Monahan EC (1990) Bubble-mediated aerosol production as a consequence of wave breaking in supersaturated (hyperoxic) seawater. J Geophys Res 95: 18281-18288.

16. Marks R (2008) Dissolved oxygen supersaturation and bubble formation in the southern Baltic Sea coastal waters. Hydrology Research 39: 229-236.

17. Monahan EC, Muircheartaigh OI (1980) Optimal power-law description of oceanic whitecap coverage dependence on wind speed. J. Physical Oceanography, 10: 2094-2099.

18. Garbalewski C, Marks R (1987) Latitudinal characteristics of aerosol distribution in the near surface air over the Atlantic. Acta Geophysica Polonica, 77-86.

19. Marks R (1990) Preliminary Investigations on the Influence of Rain on the Production, Concentration, and Vertical Distribution of Sea Salt Aerosol. Journal of Geophysical Research 95: 22299-22,304.

20. Thorpe SA (1986) Measurements with an automatically recording echo sounder; ARIES and the bubble clouds. J. Physical Oceanography 16: 1462-1478.

21. Woolf DK (1997) The Sea Surface and Global Change: Bubbles and their role in gas exchange, Liss PS and Duce RA Cambridge University Press.

22. Woolf DK, Thorpe SA (1991) Bubbles and the air-sea exchange of gases in near saturation conditions. J Marine Res 49: 435-466.

23. Cox SJ, Lipsa DR, Davies IT, Laramee RS (2013) Visualizing the Dynamics of Two-Dimensional Foams with FoamVis, Colloids and Surfaces A: Physicochemical and Engineering Aspects, 438, 28-32.

24. Miller SL, Urey HC (1959) Organic compound synthesis on the primitive earth. Science 130: 245-251.

25. Marks R, Kruczalak K, Jankowska K, Michalska M (2001) Bacteria and fungi in air over the Gulf of Gdansk and Baltic Sea. J. Aerosol Science 32: 237-250.